Applied Catalysis B: Environmental 123–124 (2012) 229–240

Contents lists available at SciVerse ScienceDirect

Applied Catalysis B: Environmental

journal homepage: www.elsevier.com/locate/apcatb

Low-temperature selective catalytic reduction of NO_x with NH_3 over Mn-containing catalysts

M. Stanciulescu*, G. Caravaggio, A. Dobri, J. Moir, R. Burich, J.-P. Charland, P. Bulsink

Natural Resources Canada, CanmetENERGY, Ottawa, Ontario K1A 1M1, Canada

ARTICLE INFO

Article history:
Received 15 November 2011
Received in revised form 30 March 2012
Accepted 6 April 2012
Available online 2 May 2012

Keywords:
NH_3–SCR for NO_x
Mn exchanged zeolites
Mn/(γ-Al_2O_3-TiO_2)
Ce/MnCBV-2314
Fe/MnCBV-2314
Cu/MnCBV-2314
Low temperature SCR

ABSTRACT

Mn-containing catalysts exhibit a high NO_x conversion in selective catalytic reduction (SCR) with NH_3. Their high activity (80–100%) covers a broad temperature range (195–600 °C). 100% N_2 formation is reached at about 230 °C for the catalysts prepared by Mn ion-exchanged in CBV-2314, a MFI zeolite. The catalysts obtained by Mn- or Fe-exchange zeolites are superior for N_2 formation compared to those prepared by wet impregnation of Mn precursors on the γ-Al_2O_3 (80%)-TiO_2 (20%) catalyst support.

Since the Mn catalysts are active for NO_x reduction in the intermediate temperature range of diesel engine exhaust mainly, an effort was undertaken in this study to extend this temperature range by promoting Mn with Cu, Ce and Fe oxides. These catalysts with two metals in the active phase were prepared and tested for DeNO$_x$ activity. All promoted catalysts showed higher formation of N_2 at either low or high temperatures. The Ce/MnCBV-2314 catalyst was more active and stable at high temperatures, close to 600 °C, than those containing Fe or Cu oxides. Cu/MnCBV-2314 showed high activity at low temperature. 100% N_2 formation for 2.1Mn/3.8FeCBV ranged from 220 to beyond 450 °C.

1. Introduction

NO_x emitted by the transportation sector contributes to more than half of the total NO_x emissions in the atmosphere. They are a significant source of air pollution, which lead to photochemical smog and acid rain, and further contribute to ozone depletion and greenhouse gases (GHG) due to the formation of N_2O. Due to climate change concerns, there is an imperative need to reduce GHG. This can be accomplished through the use of lean-burn engines, i.e. with an excess O_2 over the stoichiometric ratio, that offer significant improvement in fuel efficiency and consequently emit less CO_2. In lean-burn conditions, the regular three way catalysts cannot be used. Consequently, new technologies need to be developed to efficiently reduce NO_x under excess of O_2 without reducing engine fuel efficiency. Among these new technologies, catalytic approaches for NO_x emission control have been extensively applied to stationary and transportation sectors.

In the transportation sector, there are two main catalytic methods that are used to reduce NO_x from diesel exhaust: selective catalytic reduction (SCR), and NO_x storage reduction (NSR). The two methods have been extensively reported for more than 25 years [1]. The SCR method requires a reducing agent, which is continuously supplied in the exhaust gas to selectively react with NO_x in the presence of a catalyst converting it to N_2. Several types of reductants can be used for the SCR method, such as urea/ammonia (NH_3–SCR) [2,3], hydrocarbons (HC-SCR) [4–6], hydrogen and carbon monoxide (H_2, CO-SCR) [7,8]. Urea is convenient for on-board use as a liquid carrier for ammonia. Similarly, fuel can be used as a source of hydrocarbons, or reformed to produce CO and H_2. The NSR method consists of the oxidation of NO to NO_x over noble metals during long lean-burn engine cycles, followed by the storage of the NO_x as nitrites or nitrates on a storage component of alkaline or alkali earth compounds. The saturated storage system is then exposed to a short rich cycle that releases the stored NO_x compounds and subsequently converts them to N_2 [9,10].

One example of combining the SCR and NSR methods is reported by Lindholm et al. [11]. The ammonia formed during the rich cycle of NSR is the source of reductant for the SCR catalyst with the optimum NO_x reduction occurring at a temperature near 300 °C [11].

The reduction of NO_x at low temperatures is always important for cold start engine operations. Mn oxides are reported to have SCR activity at lower temperatures than other metal oxides [12,13]. One important parameter of the Mn catalysts to consider is the amount of Mn or Mn oxides loaded on a support. For this reason, various supports with different Mn loading capacities have been investigated, such as zeolites [14,15], TiO_2 [16–18], silica [19], mixed oxides [20,21] or activated carbon/ceramic [13].

According to many reports in the literature, it has been shown that the addition of a second metal to catalytic systems can significantly improve their activity. For example, when Fe was added to a manganese/titania catalyst, the dispersion of the manganese increased greatly which led to better NO_x conversion [16].

* Corresponding author. Tel.: +1 613 943 0103; fax: +1 613 996 9400.
E-mail address: mstanciu@nrcan.gc.ca (M. Stanciulescu).

0926-3373/$ – see front matter.
http://dx.doi.org/10.1016/j.apcatb.2012.04.012

The first objective of this study was to select the optimum Mn concentration for maximum N_2 formation from NO_x reduction by NH_3–SCR. For this purpose, several catalysts with varying concentrations of Mn (0.5–3.5 wt.%) exchanged into CBV-2314 (ZSM-5 with a silica to alumina molar ratio equal to 23) were prepared and tested. The highest Mn concentration obtained corresponded to the exchange saturation.

The second objective was to improve the Mn-zeolite activity at low and high temperatures by adding a second metal to the catalyst. The combination of the two metals was accomplished by Mn exchange on CBV-2314 and then the addition of a second transition metal by incipient wetness impregnation (IWI) of the aqueous solution of metal salt precursors. Also, the activity of these Mn catalysts was compared to the activity of catalysts prepared by IWI of γ-Al_2O_3 (80%)-TiO_2 (20%) with the same Mn precursor.

The final objective was to compare the activity of Mn ion-exchanged CBV-2314, with Fe ion-exchanged CBV-2314 promoted by Fe or Mn, respectively. All catalysts were tested for NO_x reduction using a synthetic diesel exhaust gas mixture and NH_3 as reductant.

2. Experimental

2.1. Catalyst preparation

2.1.1. Mn or Fe exchanged in NH_4CBV-2314

The zeolite NH_4CBV-2314 (NH_4ZSM-5, S_{BET} = 400 m^2/g) was supplied by Zeolyst International and used in the NH_4^+ form. All metal nitrates were purchased from Sigma–Aldrich; purities as follow: $Mn(NO_3)_2{\cdot}xH_2O$ 99.99+%, $Fe(NO_3)_3{\cdot}9H_2O$ 99.99+%, $Ce(NO_3)_3{\cdot}6H_2O$ 99.999%, $Cu(NO_3)_2{\cdot}xH_2O$ 99.99%.

Five hundred milliliter of a diluted aqueous solution of Mn(II) or Fe(III) nitrate (1.8×10^{-3} M) was mixed with NH_4CBV-2314 (7.5 g) under vigorous stirring in a refluxing flask. When the dispersion of the zeolite was completed, the temperature was increased to 85 °C and the mixture was left to stir for 5 h. The temperature was then slowly decreased to room temperature and the mixture was aged for 16 h, filtered and washed with 500 mL of de-ionized (DI) water. The collected solid was dried for 16 h at 120 °C and then calcined at 550 °C for 6 h under a stream of air. By performing repeat exchanges, a series of catalysts with increasing Mn or Fe contents, ranging in mass percentage from 0.5 to 3.5 wt.% was produced.

2.1.2. Transition metal loadings on MnCBV-2314

An aqueous solution of the transition metal precursor Cu(II), Ce(III) or Fe(III) was loaded by IWI technique on MnCBV-2314. The concentration of the transition metal (Cu, Ce or Fe) in solution was calculated to yield 3 wt.% in the final product. The wet solid was dried for 16 h at 120 °C and calcined at 550 °C for 6 h under a stream of air. The same procedure was used to impregnate transition metals on FeCBV-2314.

2.1.3. Mn oxides formation on γ-Al_2O_3 (80%)-TiO_2 (20%)

γ-Al_2O_3 (80%)-TiO_2 (20%) prepared in our laboratory [22] was loaded with a Mn(II) nitrate solution by IWI technique. The sample was dried and calcined under the same conditions used for the Mn-exchanged zeolite.

The γ-Al_2O_3 used in this experiment was prepared from aluminum isopropoxide {$Al[OCH(CH_3)_2]_3$} (AIP) (108 g) and hexylene glycol (2-methyl pentane-2,4-diol) [$(CH_3–CHOH–CH_2–C(OH)(CH_3)_2$] (120 g). The two reagents were mixed, heated and stirred at 120 °C for 4 h. The temperature was reduced to 100 °C and 90 mL of DI water was added under vigorous mixing. The mixture was stirred for an additional 2 h and subsequently the supernatant was removed by distillation. This procedure is a modified sol–gel method published by Maunula et al. [23].

The dried and calcined γ-Al_2O_3 sol–gel was covered with a monolayer of TiO_2 by using Ti isopropoxide {$Ti[OCH(CH_3)_2]_4$}(TIP) diluted in dry chromatographic-grade isopropanol. TIP (23.39 g) was added to a suspension of γ-Al_2O_3 (26.30 g) in isopropanol (200 mL) and stirred for 5 h at room temperature. After the addition of DI water (20 mL), the mixture was stirred for 16 h (overnight), dried and calcined at 500 °C for 6 h to yield a white powder. Macleod et al. published a similar method to disperse TiO_2 10% on γ-Al_2O_3 with a surface area of 120 m^2/g [8]. The chemicals used in this synthesis were purchased from Sigma–Aldrich; purities as follow: AIP 99.99+%, 2-methyl pentane-2,4-diol 99+% and TIP 97%.

2.2. Catalyst characterization

2.2.1. Surface area

The BET surface area of the catalysts was measured using a Micromeritics ASAP 2020 instrument. Each sample was degassed for 16 h at 250 °C before the isotherms were measured by standard nitrogen adsorption at −196 °C.

2.2.2. SEM/EDX

Sample compositions were determined using a Hitachi S3400 N VP-SEM fitted with an Oxford INCA EDX detector system operating at 20 kV and 80 mA. Preparation consisted of spreading a thin layer of powdered sample on a double sided carbon tape glued to a circular sample holder (13 mm diameter). The excess powder was blown off with a gentle stream of nitrogen. For each sample, a measurement was taken at ten random locations chosen by the INCA automation software. An average and standard deviation of the measurements were calculated to determine the final composition of the samples.

2.2.3. XRD

X-ray powder diffraction patterns were recorded on a Siemens D500TT automated diffractometer over the angular range 5–95° 2θ in steps of 0.02°. The XRD system was operated in the θ:θ geometry, employed Cu Kα radiation (λ = 1.5405981 Å), and was equipped with a diffracted-beam graphite monochromator, a scintillation detector and solid-state counting electronics. The XRD data were processed using JADE Plus version 7.5 software.

2.2.4. XPS

The oxidation states of the metal catalysts were analyzed by X-ray photoelectron spectroscopy (XPS) using a Kratos Axis Ultra X-ray photoelectron spectrometer. The surface of each sample was probed to a depth of 7–10 nm with the detection limits ranging from 0.1 to 0.5 at.% depending on the element. Survey scan analyses were carried out over an area of 300 μm × 700 μm using a pass energy of 160 eV. High resolution analyses were carried out over an area of 300 × 700 μm using a pass energy of 20 eV. All high-resolution spectra are charge-corrected to the main line of the C 1s signal set to 284.8 eV.

2.3. Catalyst testing

The catalysts were tested in a fixed bed flow reactor system consisting of a vertical quartz tube enclosed in a temperature-controlled furnace as shown in Fig. 1 [22]. Each sample was ground to a fine powder and then pressed into thin (~1 mm) wafers under 7 tons of pressure. After lightly crushing these wafers with a mortar and pestle, the particles were sieved within a size range of 80–120 mesh. The particles (~500 mg) were then loaded into a

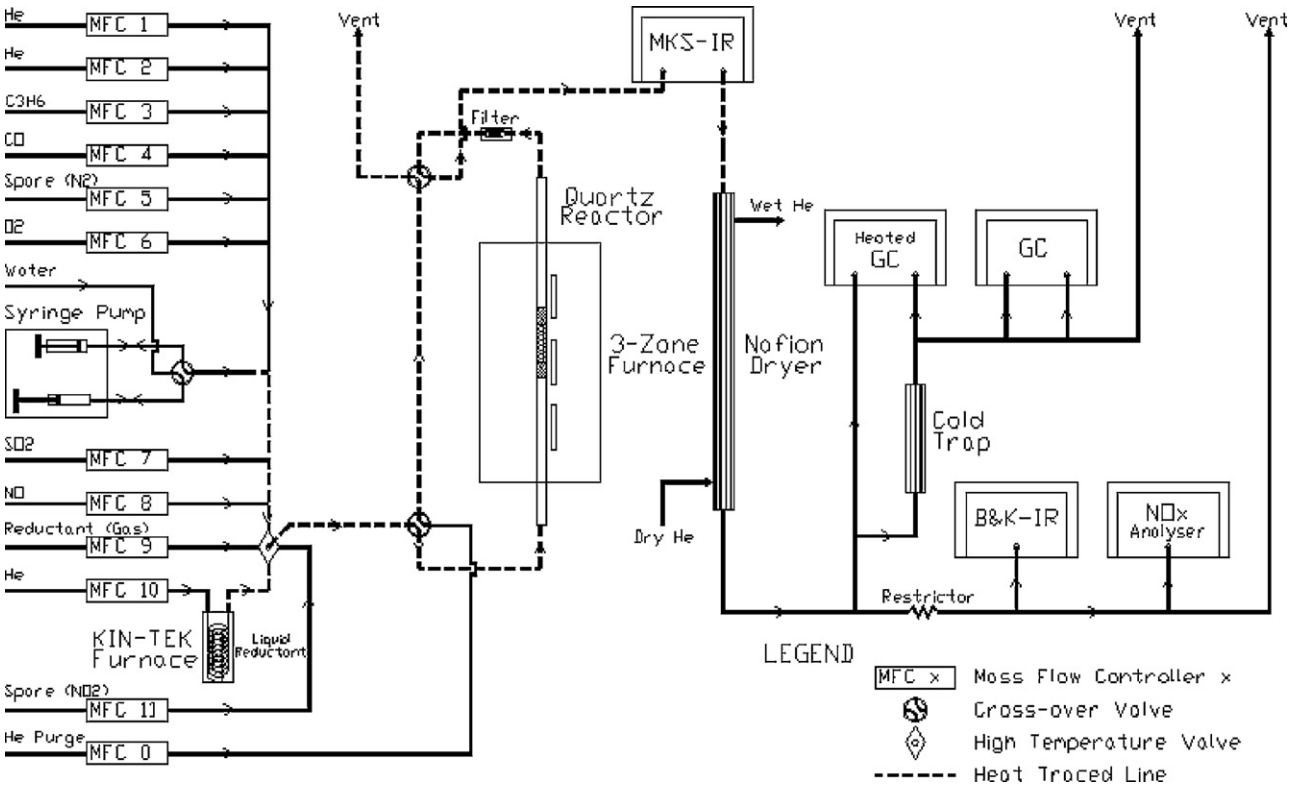

Fig. 1. Reactor system and furnace of CTU.

quartz reactor tube (6.12 mm nominal ID × 406.4 mm long) yielding a typical catalyst bed length of 26 mm. All catalytic experiments were done at a gas hourly space velocity (GHSV) ~80,000 h^{-1} [standardized to 20 °C and 1 atm] based on the catalyst volume minus the volume occupied by the thermocouple. The small variations of GHSV (~5%) were due to different catalysts densities. The feed consisted of 500 ppmv NH_3, 500 ppmv NO, 5% O_2, 5% H_2O, traces of NO_2 (<2 ppmv) with a He balance at a flow rate of 1000 mL/min standardized to 20 °C and 1 atm.

Detailed descriptions of catalyst testing and a schematic of the catalyst testing unit (CTU) were reported previously [22,24]. The temperature was ramped from 75 to 375 °C at 1 °C/min, followed by a ramp from 375 to 450 °C at 2 °C/min and to 600 °C at 3 °C/min. NO_x concentrations were monitored by a Thermo Environmental model 42H Chemiluminescence NO_x analyzer. Two on-line gas chromatographs MTI (M200 and M200H), an FTIR unit (Innova 1301 photoacoustic FTIR spectrometer) and a MKS Multigas 2030 Analyzer monitored the reactant and product gas composition continuously. The two gas chromatographs have four different columns (two per each chromatograph) for specific component separation and calibration. The M200H has a heated injection port, which prevents the condensation of high molecular weight hydrocarbons and allows their identification. The Innova 1301 photoacoustic FTIR spectrometer is used to verify the data from the MKS Multigas 2030 Analyzer, especially where adsorption overlaps occur. The placement of instruments is shown in Fig. 1.

The hydrothermal stability of some catalysts was evaluated in the CTU using a simulated diesel engine exhaust gas, containing 10% H_2O for a maximum of 100 h at various temperatures: 600, 700 and 750 °C. To estimate catalyst sulfur poisoning, SO_2 (25 ppm) was added to the simulated exhaust gas when a 600 °C hydrothermal test was performed.

3. Results and discussion

3.1. Surface area, SEM/EDS, XRD and XPS

Catalysts prepared by the ion exchanged method with the same zeolite were named according to their metal content as measured by SEM/EDX and the support name (e.g., 3.5MnCBV). For the catalysts obtained by IWI, the names also indicate the metal content as measured by SEM/EDX and the supports used for their preparation [e.g., 8.2Mn/Al_2O_3-TiO_2, or (0.9Mn + 0.9Fe)/CBV, or 2.8Cu/MnCBV]. The backslash, in the catalysts names, indicates the metals were loaded by IWI. The support γ-Al_2O_3 (80%)-TiO_2 (20%) is simplified to Al_2O_3-TiO_2 in the names of catalysts.

In general, catalyst surface area as shown in Tables 1–5 is not substantially affected by the metal loadings for the zeolitic substrate and varies from 342 to 366 m^2/g. However, for alumina-titania based catalysts, the surface area varies from 195 to 292 m^2/g. The commercial zeolite calcined at 550 °C and γ-Al_2O_3 sol–gel calcined at 500 °C, have a surface area of 352 and 292 m^2/g, respectively. The surface area of the 2.2Fe/7.4Mn/Al_2O_3-TiO_2 catalyst was the most affected, as shown in Table 2. In addition, Table 2 reveals that metals impregnated on Al_2O_3-TiO_2 do not affect the Ti percentage, but shows a small variation of Al percentage. However, the variation is small and may be due to experimental measurement errors and metal percentage calculation.

The Si/Al molar ratios for the zeolitic catalysts were calculated and are listed in Table 1 and Tables 3–5. As there is little variation from the expected value of 11.5 (as rated by the manufacturer), it appears that the ion-exchange has not compromised the structural framework of the zeolite (i.e., no Al leaching has occurred). Also, no significant variation occurs with increasing exchange; this is further evidence that no structural degradation

Table 1
Characterization of MnCBV catalysts.

Catalyst name	Metal concentrations by SEM/EDX (wt.%)				Surface area (m^2/g)	Pore volume (cm^3/g)	Pore diameter (Å)
	Mn	Si	Al	Si/Al			
CBV-2314	0	43.0	3.6	11.9	352	0.17	21.3
0.5 MnCBV	0.5	43.2	3.6	12.0	361	–	–
1.6 MnCBV	1.6	42.6	3.5	12.2	344	–	–
1.9 MnCBV	1.9	42.5	3.5	12.1	360	–	–
2.2 MnCBV	2.2	41.9	3.5	12.0	362	–	–
2.5 MnCBV	2.5	42.3	3.4	12.4	366	0.19	21.4
2.8 MnCBV	2.8	41.9	3.6	11.6	345	0.19	21.8
3.0 MnCBV	3.0	40.7	3.5	11.6	352	–	–
3.2 MnCBV	3.1	41.7	3.5	11.9	347	–	–
3.5 MnCBV	3.5	41.4	3.4	12.2	342	–	–

Table 2
Characterization of Mn/γ-Al_2O_3–TiO_2 catalysts.

Catalyst name	Metal nominal concentrations or by SEM/EDX (wt.%)						Surface area (m^2/g)	Pore volume (cm^3/g)	Pore diameter (Å)
	Mn	Fe	Ti	TiO_2	Al	Al_2O_3			
Al_2O_3	0	0	0	0	52.9	100	292	0.76	170
Al_2O_3-TiO_2	0	0	12.9 12[a]	20	41.5 42.3[b]	80	277	1.19	145
8.2Mn/Al_2O_3-TiO_2	8.2	0	12.8	–	36.0	–	220	0.78	141
9.7Mn/Al_2O_3-TiO_2	9.7	0	13.6	–	34.3	–	219	–	–
2.2Fe/7.4Mn/Al_2O_3-TiO_2	7.4	2.2	12.7	–	35.3	–	195	0.47	96.5

[a] Calculated Ti which corresponds to 20.05% TiO_2 in γ-Al_2O_3-TiO_2.
[b] Calculated Al which corresponds to 80.01% Al_2O_3 in γ-Al_2O_3-TiO_2.

Table 3
Characterization of Mn bimetallic active phase catalysts.

Catalyst name	Metal concentrations by SEM/EDX (wt.%)							Surface area (m^2/g)	Pore volume (cm^3/g)	Pore diameter (Å)
	Mn	Fe	Ce	Cu	Si	Al	Si/Al			
CBV-2314	0	0	0	0	43.0	3.6	11.9	352	0.17	21.3
3.0Fe/2.8MnCBV	2.8	3	0	0	39.5	3.3	12.0	266	0.15	23.3
0.6Ce/1.7MnCBV	1.7	0	0.6	0	42.4	3.4	12.5	–	–	–
1.0Ce/2.3MnCBV	2.3	0	1	0	41.9	3.5	12.0	–	–	–
2.9Ce/2.8MnCBV	2.8	0	2.9	0	40.5	3.4	11.9	327	0.18	21.8
2.8Cu/2.8MnCBV	2.8	0	0	2.8	40.5	3.4	11.9	297	0.16	22.1

Table 4
Characterization of other Mn catalysts.

Catalyst name	Metal concentrations by SEM/EDX (wt.%)							Surface area (m^2/g)	Pore volume (cm^3/g)	Pore diameter (Å)
	Mn	Fe	Ce	Pd	Si	Al	Si/Al			
CBV-2314	0	0	0	0	43.0	3.6	11.9	352	0.17	21.3
(0.9Mn + 0.9Fe)/CBV	0.9	0.9	0	0	42.5	3.6	11.8	295	0.09	11.5
(0.7Mn+ 0.5Pd)/CBV	0.7	0	0	0.5	42.4	3.6	11.8	353	0.18	20.3

Table 5
Characterization of Fe catalysts.

Catalyst name	Metal concentrations by SEM/EDX (wt.%)							Surface area (m^2/g)	Pore volume (cm^3/g)	Pore diameter (Å)
	Fe	Mn	Pd	Ce	Si	Al	Si/Al			
CBV-2314	0	0	0	0	43.0	3.6	11.9	352	0.17	21.3
1.4FeCBV	1.4	0	0	0	42.7	3.5	12.2	–	–	–
3.2FeCBV	3.2	0	0	0	41.9	3.3	12.7	350	–	–
3.5FeCBV	3.5	0	0	0	41.9	3.1	13.5	–	–	–
4.1FeCBV	4.1	0	0	0	41.6	3.1	13.4	–	–	–
0.9 Mn3.3FeCBV	3.3	0.9	0	0	41.3	3.4	12.1	356	0.20	22.6
2.1Mn/3.8FeCBV	3.8	2.1	0	0	40.3	3.3	12.2	329	0.19	23.5
1.4Mn/4.1FeCBV	4.1	1.4	0	0	40.6	3.3	12.3	325	0.18	22.1
4.0Ce/3.0FeCBV	3.0	0	0	4	39.8	3.2	12.4	360	–	–
1.1Pd/3.2FeCBV	3.2	0	1.1	0	41.3	3.4	12.1	354	0.201	22.7
1.5Pd/3.9FeCBV	3.9	0	1.5	0	40.7	3.3	12.3	345	0.195	22.6

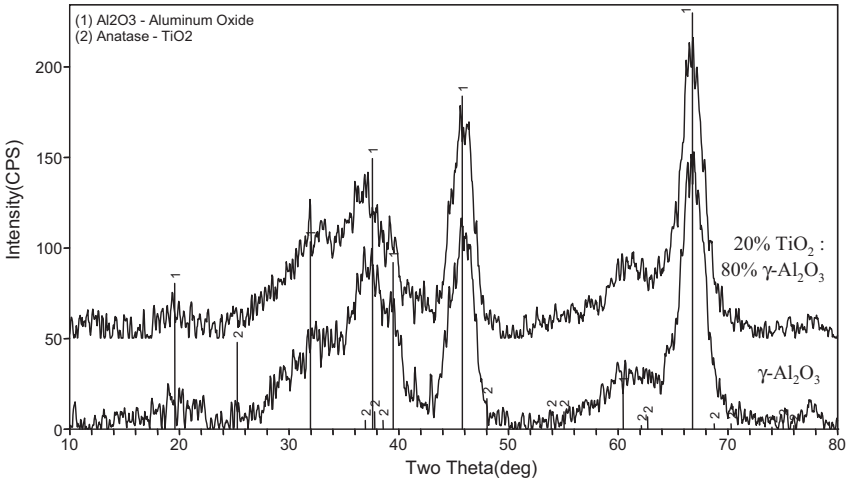

Fig. 2. XRD spectra of γ-Al_2O_3 and γ-Al_2O_3 (80 wt.%)-TiO_2 (20 wt.%).

of the support occurred. Table 3 shows the characteristics of the Mn ion-exchanged CBV-2314 catalysts loaded with one additional metal by using the IWI technique via an aqueous solution of Fe, Ce or Cu nitrate. The catalyst 3.0Fe/2.8MnCBV has the lowest surface area, compared to the other zeolitic catalysts loaded with two metals. Table 4 shows the characteristics of the catalysts prepared by concomitant IWI of two metals as nitrate precursors. The presence of Fe affects the surface area and the pore size of the catalyst. The pore size of the (Mn + Fe)/CBV catalyst is almost half of that of CBV or (Mn + Pd)/CBV. However, if Fe is ion-exchanged in the zeolite, the surface area is not severely changed compared to that of the initial zeolite (Table 5). This may be due to better dispersion of Fe occurring by ion-exchange compared to Fe being impregnated on the zeolite.

The metal content measured by SEM/EDX is in good agreement with the nominal loadings for the catalysts loaded by IWI. The standard deviations corresponding to the metal compositions of the catalysts prepared with the alumina-titania support are higher (max. 0.6) compared to those on the zeolite support (<0.1), but on a percentage basis these deviations are comparable.

The X-ray diffraction patterns of γ-Al_2O_3 prepared by the sol–gel technique and the γ-Al_2O_3 (80%)-TiO_2 (20%) catalyst support are shown in Fig. 2.

The sample containing 20 wt.% TiO_2 displayed a XRD pattern identical to that of the γ-Al_2O_3 support, indicating that the TiO_2 component was highly dispersed over the surface of the alumina. Given the surface area of our starting γ-Al_2O_3 (270 m^2/g), a calculation based on the crystal structure parameters of anatase suggests that a monolayer coverage could still be achieved by coating this γ-Al_2O_3 with up to approximately 20 wt.% TiO_2.

High-resolution XPS spectra for Mn 2p of Mn compounds from various catalysts show values for binding energy starting at 640.4–646.6 eV (Table 6). The catalysts obtained by ion exchange contain Mn^{2+}, Mn^{3+}, and Mn^{4+} compounds. Table 6 shows the concentrations of Mn species in 1.6 MnCBV (~53% MnO, ~19% Mn_2O_3 and ~28% MnO_2) and in 2.2MnCBV (~16% MnO, 72% Mn_2O_3 and 12% MnO_2). The catalyst 9.7Mn/Al_2O_3-TiO_2 loaded by wet impregnation with an excess of water (~10% more water than that used for 8.2Mn/Al_2O_3-TiO_2 loaded by IWI) contains two Mn compounds, ~57% Mn_2O_3 and ~43% MnO_2 (Fig. 3a), differing from

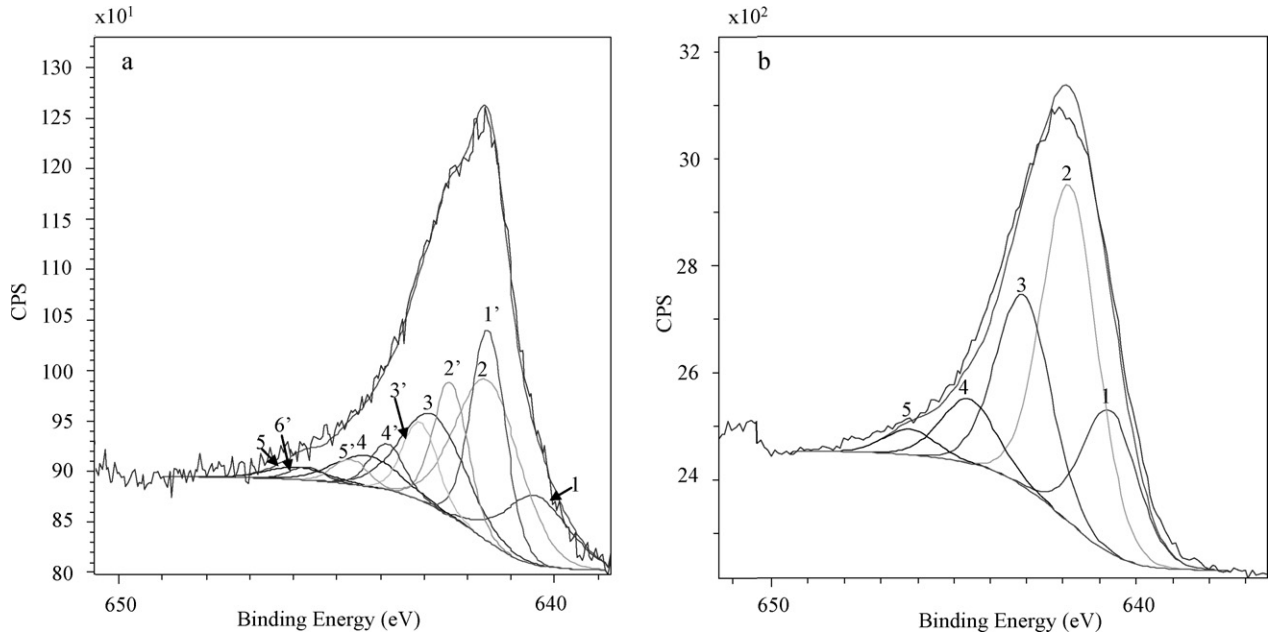

Fig. 3. Mn 2p high-resolution XPS spectra; (a) 9.7Mn/Al_2O_3-TiO_2 [Mn(III) peaks 1–5; Mn(IV) peaks 1′– 6′); (b) 8.2Mn/Al_2O_3-TiO_2 [Mn(III) peaks 1–5].

Table 6
Mn2p, high-resolution XPS spectra fitting parameters: binding energy (eV), percentage of total area, FWHM values (eV) for each pass energy.

Catalyst	Compound detected	Peak #	Energy (eV)	FWHM (eV)	Area (%)
1.6MnCBV	Mn_2O_3	1	641.03	1.73	18.9
		2	642.15	0	0.0
		3	643.12	0	0.0
		4	644.70	0	0.0
		5	646.78	0	0.0
		6	646.83	0	0.1
	MnO_2	1	641.76	0.93	25.4
		2	642.40	0.93	1.2
		3	643.43	0	0
		4	644.05	0.93	0.6
		5	644.70	0.93	0.7
	MnO	1	640.49	1.25	23.1
		2	641.47	1.25	29.9
2.2MnCBV	Mn_2O_3	1	640.84	1.73	6.9
		2	642.15	1.73	31.0
		3	643.12	1.73	22.2
		4	644.68	1.73	6.5
		5	644.70	1.73	0.0
		6	646.78	1.60	4.9
	MnO_2	1	641.86	0.93	0.6
		2	641.73	0.93	0.3
		3	643.43	0.93	0.2
		4	643.88	0.93	8.4
		5	644.71	0.93	0
		6	645.76	0.93	2.8
	MnO	1	640.00	1.25	1.4
		2	641.35	1.25	14.9
9.7Mn/Al_2O_3-TiO_2	Mn_2O_3	1	640.43	1.73	25.4
		2	641.53	1.73	14.4
		3	642.80	1.73	4.8
		4	644.30	1.73	2.1
		5	645.92	1.60	1.8
	MnO_2	1	641.53	0.93	17.8
		2	642.39	0.93	11.3
		3	643.09	0.93	6.6
		4	643.84	0.93	3.9
		5	644.69	0.93	2.1
		6	645.69	0.93	1.1
8.2Mn/Al_2O_3-TiO_2	Mn_2O_3	1	640.72	1.77	18.9
		2	641.82	1.77	44.4
		3	643.09	1.77	25.2
		4	644.59	1.77	8.5
		5	646.21	1.60	3.1
2.1Mn/3.8FeCBV	Mn_2O_3	1	640.99	1.77	14.7
		2	642.09	1.77	34.5
		3	643.36	1.77	19.6
		4	644.86	1.77	6.6
		5	646.48	1.60	2.4
	MnO	1	640.39	1.25	5.3
		2	641.36	1.25	6.2
		3	642.29	1.25	4.9
		4	643.24	1.25	2.8
		5	644.38	1.25	1.0
		6	646.13	1.25	2.0
2.8Cu/2.8MnCBV	Mn_2O_3	1	641.10	1.77	18.5
		2	642.20	1.77	43.6
		3	643.47	1.77	24.8
		4	644.97	1.77	8.3
		5	646.59	1.60	3.0
	MnO_2	1	642.20	0.89	0.8
		2	643.06	0.89	0.5
		3	643.76	0.89	0.3

8.2Mn/Al_2O_3-TiO_2 that contains 100% Mn(III) as Mn_2O_3 (Fig. 3b). In the catalyst 2.1Mn/3.8FeCBV, the Mn is present as Mn(III) (Mn_2O_3) at ~ 85% and ~15% as Mn(II) (MnO). In the Fe-exchanged catalyst the iron is Fe(III) and appears as γ-Fe_2O_3 (~63%) and FeOOH (~36%) (Fig. 4 and Table 7). The curve-fitting procedure was similar to that performed by Biesinger et al. [25]. The high-resolution XPS of the metal compounds from 2.8Cu/2.8MnCBV catalyst are presented in Fig. 5 and spectral fitting parameters given in Table 6 for the Mn compounds and Table 8 for the Cu compounds. Fig. 5a is the XPS of Mn 2p with the binding energy starting at 641.1–646.4 eV corresponding to Mn(III) and Mn(IV), respectively. The peak intensities of MnO_2 are very weak, representing 2% of total peak area. Fig. 5b and c shows mixed Cu oxides with Cu(I) and Cu(II) where Cu(I) is mostly produced from catalyst exposure to X-rays. The quantification procedure for Cu species has been published by Biesinger et al. [26]. The oxidation states for the above metals have been

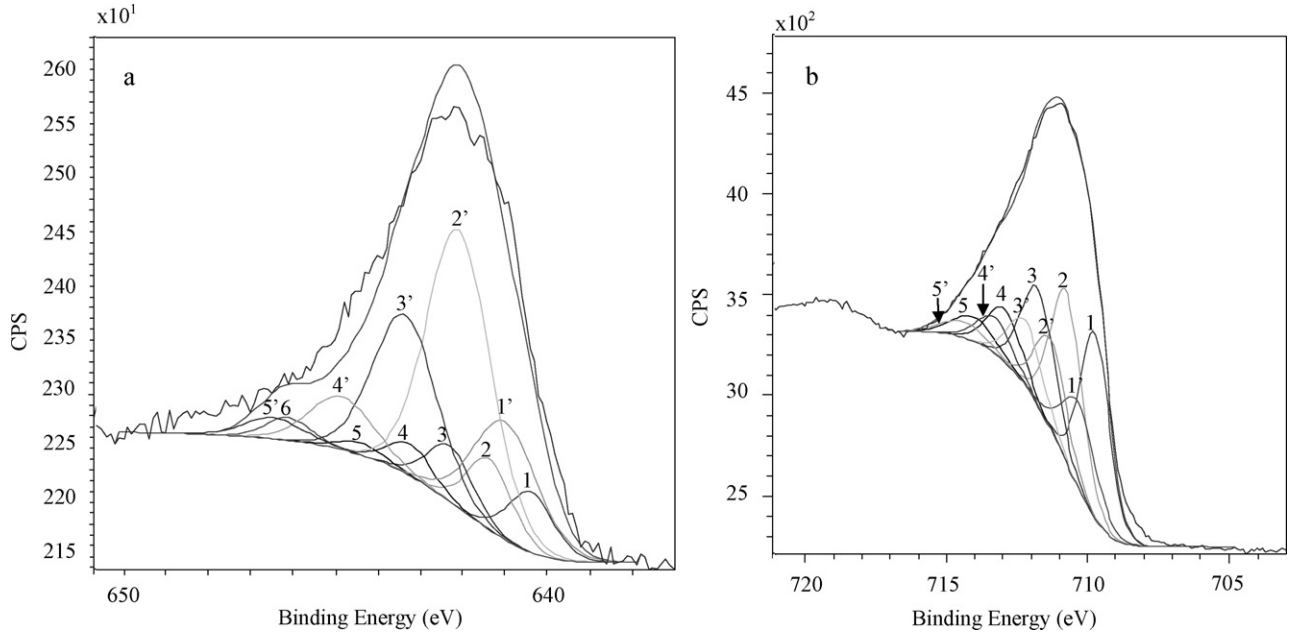

Fig. 4. High-resolution spectra of 2.1Mn/3.8FeCBV. (a) Mn 2p [peaks 1–6 Mn(II) and peaks 1′–5′ Mn(III)]; (b) Fe 2p[Fe(III) peaks: 1–5 FeOOH and peaks 1′-5′ Fe_2O_3].

compared to those reported in literature and found to be similar [17,27,28].

3.2. Catalyst $DeNO_x$ activity

The activity of catalysts in this study focused on the standard-SCR reaction involving equal amounts of NO and NH_3 in the presence of oxygen.

$$4NH_3 + 4NO + O_2 \rightarrow 4N_2 + 6H_2O \quad (1)$$

3.2.1. Effect of Mn concentration on NO_x reduction

The catalytic activity of Mn ion-exchanged zeolites increased with increasing metal content (Fig. 6) reaching a maximum NO_x conversion to N_2 (Fig. 7) at a Mn concentration of 3.5 wt.%. Some of the catalysts shown in Fig. 6 have been presented in one of our previous study [29]. Li et al. have also observed an increase of catalytic activity with increasing metal content [30]. The catalyst 3.5MnCBV corresponding to the Mn exchange saturation is the most active, reaching 100% NO_x conversion to N_2 at about 220 °C and this high activity is maintained to about 450 °C (Fig. 7). The starting zeolite with no Mn shows poor activity at low temperature, reaching 50% NO_x conversion at only 450 °C. The positive effect of low amounts of Mn is observed at about 225 °C (1.6MnCBV), but only for a short temperature interval because above 375 °C the $DeNO_x$ activity decreases below that obtained by the unloaded CBV-2314. An increased amount of Mn-exchanged in the zeolite, translates to a large increase in $DeNO_x$ activity (Fig. 6) and formation of N_2 as shown in Fig. 7. The catalyst 1.9MnCBV attained a 100% NO_x conversion plateau at about 250 °C with all NO_x being converted to N_2 (Fig. 7). All catalysts containing Mn ≥ 1.9 wt.% did not produce other by-products such as N_2O, or other NH_3

Table 7
Fe2p, high-resolution XPS spectra fitting parameters: binding energy (eV), percentage of total area, FVHM values (eV) for each pass energy.

Catalyst	Compound detected	Peak #	Energy (eV)	FWHM (eV)	Area (%)
2.1Mn/3.8FeCBV	γ-Fe_2O_3	1	709.75	1.20	19.7
		2	710.75	1.30	19.7
		3	711.75	1.40	14.6
		4	712.95	1.40	6.5
		5	714.05	1.70	3.7
	FeOOH	1	710.30	1.40	10.5
		2	711.30	1.30	10.3
		3	712.20	1.40	8.0
		4	713.30	1.40	4.5
		5	714.40	1.80	2.4

Table 8
Cu2p high-resolution XPS spectra fitting parameters: binding energy (eV), percentage of total area, FVHM values (eV) for each pass energy.

Catalyst	Compound detected	Peak #	Energy (eV)	FWHM (eV)	Area (%)
2.8Cu/2.8MnCBV	Cu oxid	1	933.56	1.64	50.0
	Long X-ray exposure	2	935.50	2.42	29.9
		3	943.62	2.62	10.3
		4	944.73	2.40	9.8
	Cu oxide	1	933.47	1.73	31.6
	Short X-ray exposure	2	935.48	2.93	37.8
		3	942.80	4.34	23.6
		4	945.18	2.28	7.0

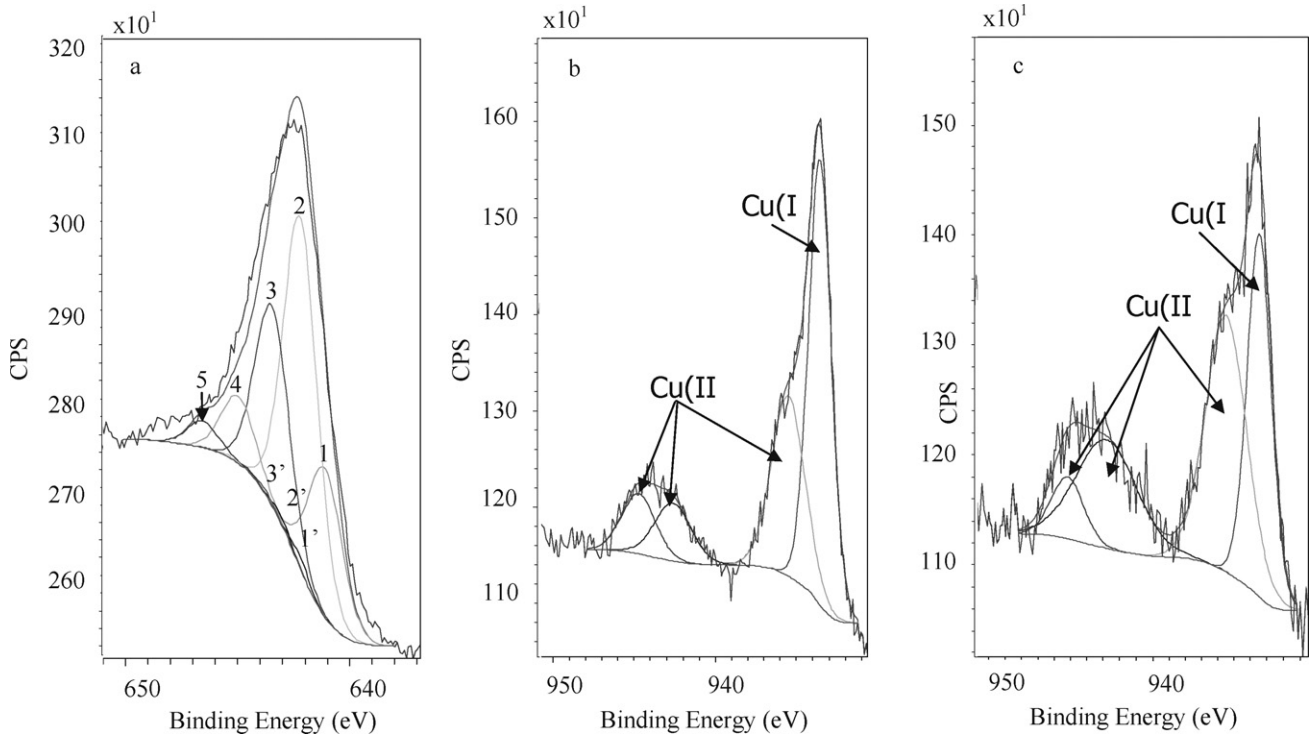

Fig. 5. High-resolution XPS spectra of 2.8Cu/2.8MnCBV: (a) Mn 2p [Mn(III) peaks 1-5 and Mn(IV) peaks 1′–3′]; (b) Cu 2p [Cu(I) and Cu(II) with long X-ray exposure]; (c) Cu 2p [Cu(I) and Cu(II) with short X-ray exposure].

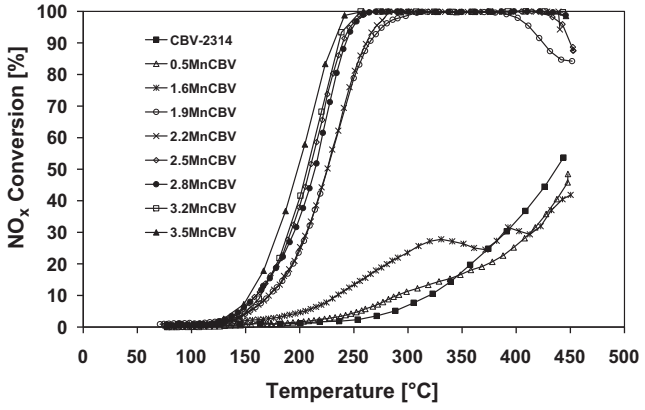

Fig. 6. Effect of the Mn content in Mn-exchanged zeolites on NO_x conversion.

oxidation products at low or high temperatures. The support, 0.5MnCBV and 1.6MnCBV produced N_2O starting at 200 °C with a maximum NO_x conversion to N_2O at 350 °C (Fig. 8). 1.6MnCBV produced the most N_2O, which is an unwanted by-product. Based on the high resolution spectra, 1.6MnCBV has a low amount of Mn^{3+} (~19%) that appears to be active for NO_x reduction, and a Mn^{3+}/Mn^{4+} ratio of ~0.7. In contrast, 2.2MnCBV has a higher amount of Mn^{3+} (~72%), a Mn^{3+}/Mn^{4+} ratio of ~6 and much higher $DeNO_x$ activity and no formation of by-products. 1.6MnCBV is active for the reduction of NO_x only for a short temperature interval. At about 370 °C, the activity slightly increased suggesting a reactivation of the catalyst surface. Furthermore, the Mn amount contained in 1.6MnCBV is too low for making durable $DeNO_x$ catalysts for NH_3–SCR. Our previous study on MnCBV catalysts correlated the increased of Mn concentration to higher NH_3 adsorption on the metallic surface due to increased amounts of Lewis acid sites [29]. In addition, Palomares et al. found that the combination of

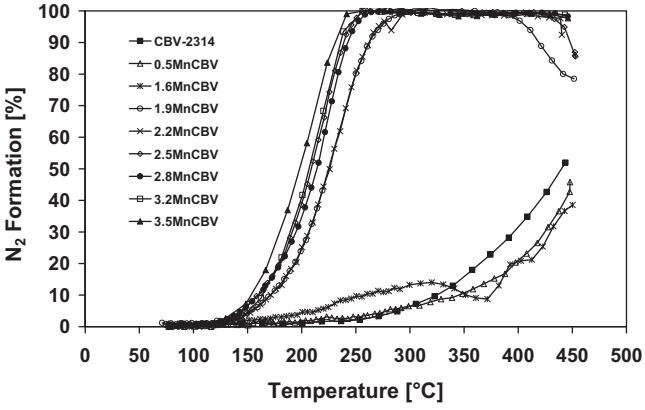

Fig. 7. Effect of the Mn content in Mn-exchanged zeolites on N_2 formation.

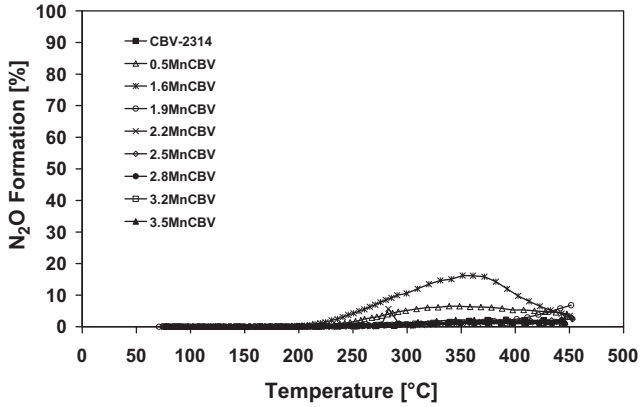

Fig. 8. Effect of the Mn content on N_2O formation.

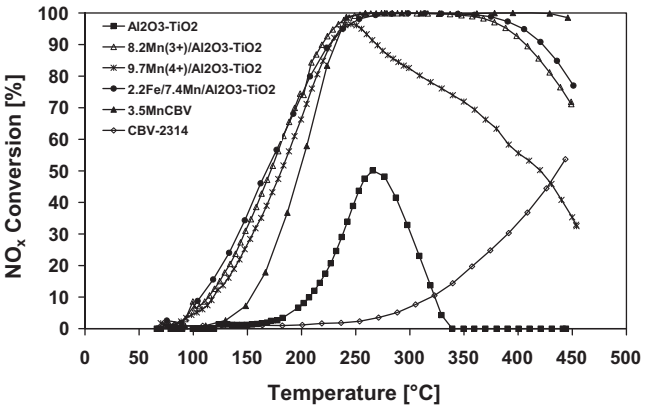

Fig. 9. Comparison of $DeNO_x$ activity of catalysts with various supports.

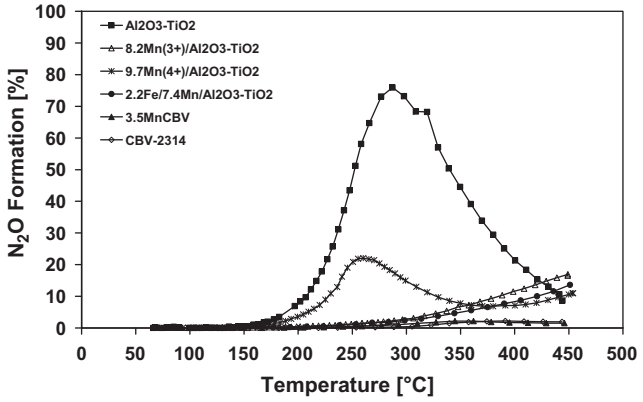

Fig. 11. Effect of catalyst support on NO_x reduction to N_2O.

Brønsted acid sites with Mn_2O_3, SnO_2 or CuO can enhance the NO_x reduction to N_2 [31].

3.2.2. Effect of the support on Mn catalytic activity

The support plays an important role in catalytic $DeNO_x$ activity. During the last decade, Mn has been loaded on various supports or tested as mixed oxides for NO_x reduction [13–21]. The $DeNO_x$ activity of various Mn-support combinations is of high interest, especially combinations of Mn oxides and modified TiO_2 [17,32].

In this study we compared Mn ion-exchanged zeolites with Mn impregnated on alumina-titania. The zeolite support introduced Brønsted acid sites (e.g. CBV-2314), and alumina-titania, oxidation sites [e.g. Al_2O_3(80%)-TiO_2(20%)]. During the calcination stage, the impregnated Mn precursor was converted to Mn oxides (Mn_2O_3 and/or MnO_2). Fig. 9 shows the conversion of NO_x using Al_2O_3-TiO_2, 8.2Mn/Al_2O_3-TiO_2, 9.7Mn/Al_2O_3-TiO_2, 2.2Fe/7.4Mn/Al_2O_3-TiO_2, 3.5MnCBV and CBV-2314(100%). The conversion of NO_x to N_2 is shown in Fig. 10. The support, Al_2O_3-TiO_2, converted NO_x to N_2O (Fig. 11) and also partially oxidized NH_3 to N_2O as indicated in equation (2).

$$2NO + 2NH_3 + 3/2O_2 \rightarrow 2N_2O + 3H_2O \quad (2)$$

The oxidation effect of Al_2O_3-TiO_2 was lowered by the deposition of Mn (Mn oxides) on its surface, converting the Mn/Al_2O_3-TiO_2 to a NO_x reduction catalyst. The catalyst 8.2Mn/Al_2O_3-TiO_2 had a high $DeNO_x$ activity at low temperature and reached 100% conversion to N_2 at 200 °C (Fig. 10). XPS analysis indicated that all Mn in this catalyst was at the oxidation state 3+. However, the 9.7Mn/Al_2O_3-TiO_2 catalyst loaded by wet impregnation, with an excess of water, contained the Mn at two oxidation states 3+ and 4+. Consequently, the latter catalyst is less active at temperatures above 250 °C compared to 8.2Mn/Al_2O_3-TiO_2. This difference in activities may be due to the double catalytic activity of Mn_2O_3. In the presence of oxygen, NO is oxidized to NO_2 and then NO_2 is reduced in the presence of a reductant to N_2 on the metallic active sites of Mn_2O_3 [31]. This corresponds to the fast-SCR reaction shown in equation (3).

$$4NH_3 + 2NO + 2NO_2 \rightarrow 4N_2 + 6H_2O \quad (3)$$

The lower $DeNO_x$ activity of 9.7Mn/Al_2O_3-TiO_2 compared to 8.2Mn/Al_2O_3-TiO_2 may be due to inactivation resulting from the formation of nitrates on the catalyst surface, as shown in the following reaction:

$$MnO_2 + N_2O_4 \rightarrow Mn(NO_3)_2 \quad (4)$$

Further, the nitrate will be decomposed to release NO_2

$$Mn(NO_3)_2 \rightarrow MnO_2 + 2NO_2 \quad (5)$$

The presence of N_2O and NO_2 in the reaction products is shown in Fig. 12. However, the reactions (2) and (3) would have to be confirmed by more experimental data (e.g. in situ FTIR to show the formation of nitrates).

The 2.2Fe/7.4Mn/Al_2O_3-TiO_2 showed a slight increase in $DeNO_x$ activity at lower temperatures in comparison to 8.2Mn/Al_2O_3-TiO_2. This may suggest a synergy between Fe and Mn resulting in improved activity. In contrast, 3.5MnCBV is more active at higher temperatures than all the other catalysts shown in Figs. 9 and 10.

3.2.3. Comparison between catalysts containing Mn ion-exchanged CBV-2314 promoted with Cu, Ce, and Fe oxides

Fig. 13 shows the conversion of NO_x in the presence of Mn ion-exchanged zeolite promoted with Cu, Ce and Fe. The concentrations

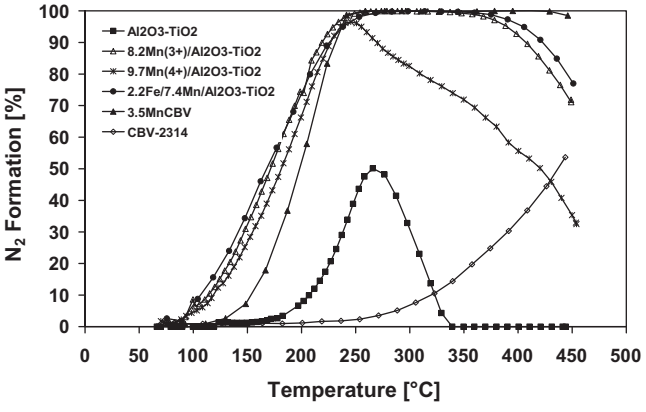

Fig. 10. Effect of catalyst support on NO_x reduction to N_2.

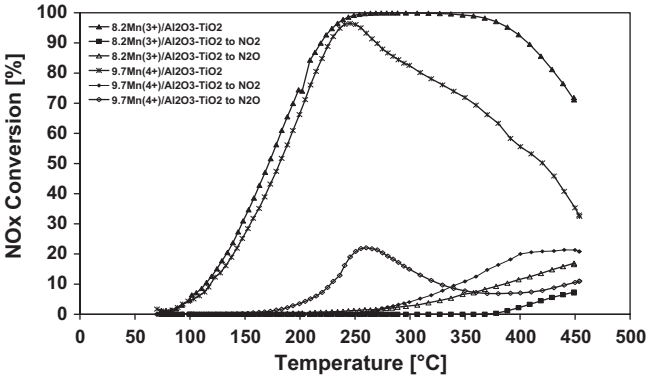

Fig. 12. Activity comparison of 8.2Mn/Al_2O_3-TiO_2 and 9.7Mn/Al_2O_3-TiO_2.

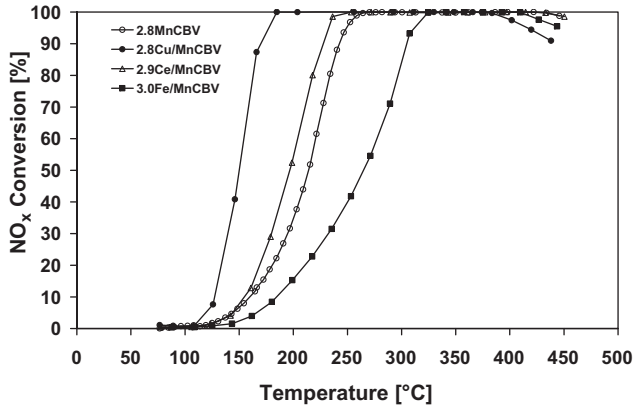

Fig. 13. Effect of the 2nd metal loaded on Mn-exchanged zeolite on NO_x reduction.

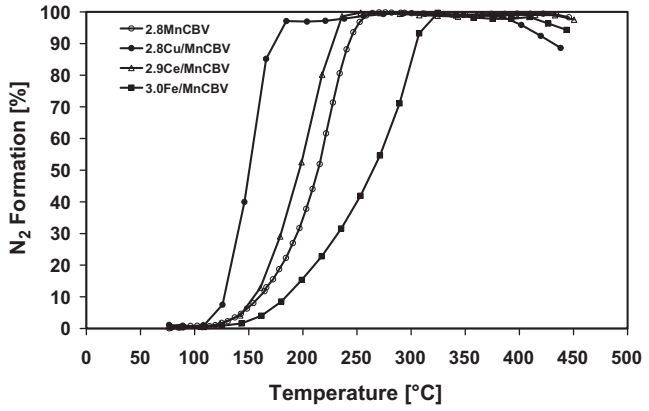

Fig. 14. Effect of the 2nd metal loaded on Mn-exchanged zeolite on N_2 formation.

of Mn, Cu, Ce and Fe varied from 2.8 to 3.0 wt.%. The presence of Cu shifted the NO_x conversion to low temperature, with 50% conversion at about 130 °C. The overall NO_x conversion measured from 75 to 600 °C was 82% for 2.8Cu/2.8MnCBV compared to 2.8MnCBV, which was 78%. Most of the Cu is at the oxidation state 2+ and only a small amount is as Cu(I). The XPS was not conclusive on the oxidation state of Cu because the long and short exposure to X-rays produced some Cu(I). Kang et al. observed similar low temperature activity when they investigated Cu-Mn mixed oxide catalysts for NO_x conversion [21].

Adding Ce to 2.8MnCBV improved the $DeNO_x$ activity slightly at low temperatures and the catalyst maintained its original NO_x conversion at higher temperatures, yielding an overall $DeNO_x$ activity of 80%. Qi and Yang found the manganese-cerium catalysts yielded nearly 100% NO_x conversion at low temperatures (about 120 °C) [33]. They concluded the addition of CeO_2 significantly improved the dispersion of the active component over the surface of the catalyst and enhanced active sites per unit area. The 2.9Ce/2.8MnCBV catalyst in this study did not reach 100% NO_x conversion at 120 °C, however, the NO_x reduction was without by-product formation. The ceria deposited on Mn-exchanged zeolite prevented the unselective oxidation of NH_3 by O_2 to N_2O, NO or NO_2. This interpretation is in agreement with what Guan et al. found in their study of catalysts containing Ce-Mn [34]. Appreciable $DeNO_x$ activity was also observed for catalysts synthesized with Ce and Mn loaded in MCM-41 mesoporous molecular sieves [35].

3.0Fe/2.8MnCBV was less active than 2.8MnCBV at low temperatures, however, it maintained its $DeNO_x$ activity at high temperatures and this resulted in an overall NO_x reduction of 65%. This decrease in activity may be due to its low surface area (Table 3). In addition, the activity of 3.0Fe/2.8MnCBV could be reduced by iron oxide deposition on exchanged manganese reducing the oxidation/reduction capacity of the latter metal and by blockage of NO iron oxidation sites by NH_3 that inhibits the standard-SCR reaction as found by Metkar et al. [36]. The three catalysts based on 2.8MnCBV converted NO_x selectively to N_2 as is shown in Fig. 14.

A comparison of Cu-containing catalysts was done to clarify the possible synergistic effect between Mn and Cu. Fig. 15 shows that the complete NO_x conversion of 2.8Cu/2.8MnCBV starts at 200 °C and continues to 384 °C. The $DeNO_x$ activity of 2.6CuCBV drops abruptly at 360 °C and shows the formation of by-products such as N_2O and NO_2. The difference in activity of the two catalysts could be due to the synergistic effect between the Cu and Mn species. Also, Fig. 15 shows the hydrocarbon effect on the 2.6CuCBV activity, by adding CH_4 and C_2H_4, (~750 ppm each) to the simulated diesel engine exhaust gases. There was no significant change in activity at low temperatures and only a small activity decrease starting at

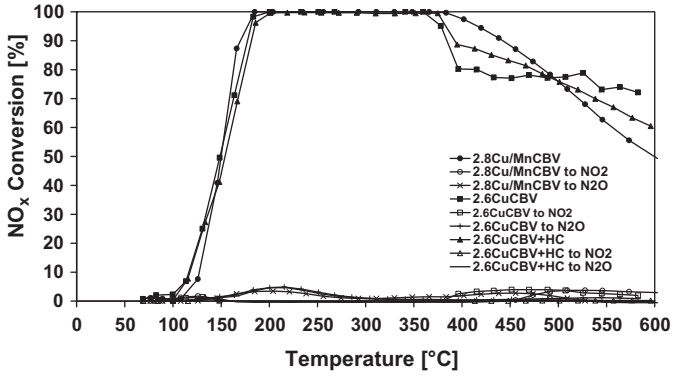

Fig. 15. Activity comparison of Cu-containing catalysts.

500 °C. The formation of by-products, N_2O and NO_2, was noticed in small amounts with or without hydrocarbons (Fig. 15).

3.2.4. Comparison of Fe ion-exchanged CBV-2314 with Mn ion-exchanged CBV-2314

Fig. 16 shows the NO_x conversion activity of Fe-exchanged zeolite (CBV-2314) promoted by a 2nd transition metal. In this series, the highest NO_x reduction was obtained with the catalyst containing Mn on Fe ion-exchanged zeolite (i.e., 2.1Mn/3.8FeCBV). The activity of 2.1Mn/3.8FeCBV approached 100% formation of N_2 at ~220 °C and maintained its conversion at high temperatures (>450 °C). Previous studies showed the introduction of Mn into Fe containing SCR catalysts, enhanced the low temperature activity. This it is probably due to the synergistic effect between iron and

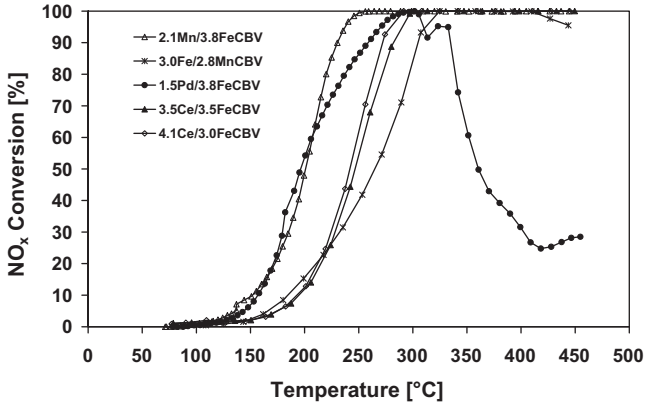

Fig. 16. Effect of 2nd metal loaded on Fe-exchanged zeolite on NO_x reduction.

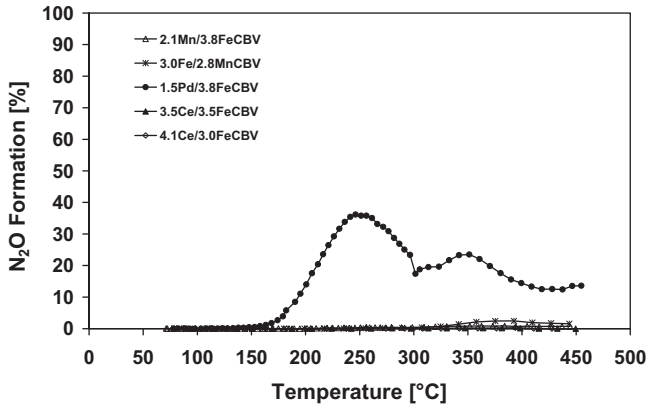

Fig. 17. Effect of 2nd metal loaded on Fe-exchanged zeolite on N_2O formation.

manganese species [37]. The addition of Mn could also enhance the Brønsted acid sites on the catalyst surface, accelerating the NH_3 adsorption at low temperatures and consequently enhance the SCR reaction [34]. The variation of Fe or Ce concentration does not have a high impact on catalyst activity.

The Pd/FeCBV catalyst shown in Fig. 16 is active at low temperature and this activity decreased rapidly at temperatures above 350 °C. However, this lack of activity is due to a significant amount of NO_x converted to N_2O (Fig. 17).

The two catalysts containing Mn and Fe on CBV have different amounts of N_2 formation (Fig. 18). This difference may be due to the order of metal loading on the zeolite. It appears the activity for N_2 formation with the catalyst 2.8MnCBV (Fig. 7) is shifted to higher temperatures when Fe is present, e.g. for 3.0Fe/2.8MnCBV (Fig. 18). The interaction between Fe ions and Mn ion-exchanged zeolite had a negative effect on the $DeNO_x$ activity of MnCBV. Ce as the second metal had an effect similar to Fe, but with lower intensity. Pd in Pd/FeCBV also shifted N_2 formation to higher temperatures compared to other catalysts as shown in Fig. 18.

3.2.5. Competition to N_2 formation

In general, Mn-containing catalysts obtained by ion exchange are active for NO_x reduction to N_2 at low temperatures (Figs. 7, 10, 14, 18). The zeolitic support, CBV-2314, reduces NO_x to N_2 only at high temperatures. Mn deposited by wet impregnation on γ-Al_2O_3(80%)-TiO_2(20%) is less selective for N_2 formation, particularly when the catalyst contains Mn(IV) (Fig. 10). The γ-Al_2O_3(80%)-TiO_2(20%) support converts a large amount of NO_x to N_2O (Fig. 11) and less to N_2. However, the catalyst containing Cu loaded as the second metal by IWI on Mn ion-exchanged zeolites (2.8Cu/2.8MnCBV) is very active for N_2 formation at low temperatures compared to 2.1Mn/3.8FeCBV which attained 100% N_2 formation at ~220 °C and continued this level of conversion beyond 450 °C. The two catalysts, 3.5Ce/3.5FeCBV and 4.1Ce/3.0FeCBV, containing different amounts of Ce and Fe have similar NO_x reduction to N_2 and are more active than the 3.0Fe/2.8MnCBV catalyst series. Pd/FeCBV is less active for N_2 formation and produces N_2O as a by-product, which is undesirable for a $DeNO_x$ catalyst.

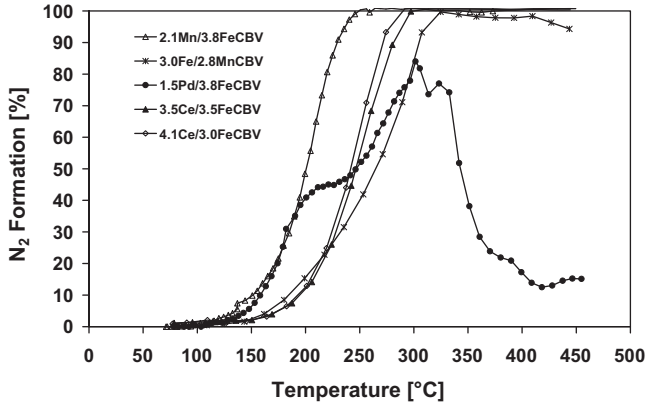

Fig. 18. Effect of 2nd metal loaded on Fe-exchanged zeolite on NO_x reduction to N_2.

3.2.6. Effect of aging on catalyst $DeNO_x$ activity

The tests performed with the regular conditions, after hydrothermal aging, indicated that the maximum activity of the catalysts was shifted to higher temperatures. Some activity of the aged catalysts was recovered by testing the catalysts with a ratio NO:NO_2 of 1:1. The observed deactivation is believed to be due to zeolite dealumination. However, zeolite $DeNO_x$ catalysts can be the subject of different other types of deactivations in addition to hydrothermal dealumination, when they are aged in diesel engine exhaust gases, such as: depositions of coke from unburned hydrocarbons and deactivation due to the heteroatoms (S, P, Zn) from engine lubricant additives. At this time, we do not have a clear answer to the long term operation and robustness of catalysts. Additional aging tests and characterization of aged catalysts need to be performed to obtain accurate information on the changed activity.

4. Conclusions

From this study, it is concluded that Mn ion-exchanged zeolite (with Mn >1.6%) are good catalysts for NO_x reduction in the presence of high oxygen concentration, using NH_3 as a reducing agent and they are therefore good candidates for NH_3–SCR of NO_x. The catalyst activity increased with the Mn concentration and reached a plateau around the maximum exchange capacity of the zeolite (~3.5%).

The catalyst containing Mn(III) appears to be more active for NO_x reduction than those with Mn(IV).

The catalysts with two metals in the active phase, based on Mn or Fe ion-exchanged zeolites are also active for NH_3–SCR of NO_x under lean-burn conditions.

The active components of the two-metal active phase catalysts, such as Cu-Mn, Fe-Mn, Ce-Mn, Mn-Fe or Ce-Fe, exist in the form of mixed-oxidation state, which was beneficial for the oxidation of NO to NO_2.

Activity of Mn ion-exchanged zeolites can be improved by adding another metal such as Cu, Ce or Fe. 2.8Cu/2.8MnCBV showed increased $DeNO_x$ activity at low temperatures and 3.0Ce/2.8MnCBV showed increased stable activity at elevated temperatures.

Good results for NO_x conversion to N_2 were also obtained with the catalysts containing Fe-exchanged zeolite and MnO_x formed on zeolite after impregnation with a Mn aqueous solution precursor and calcined in air at 550 °C.

Acknowledgments

The authors would like to thank the Government of Canada Program on Energy Research and Development (PERD) for financial support under the Advanced Fuels and Transportation Emissions Reduction (AFTER) program.

We would also like to thank Mr. K. Wittich for the final proof reading of this manuscript.

References

[1] S. Roy, M.S. Hedge, G. Madras, Applied Energy 86 (2009) 2283–2297.

[2] M. Takagi, T. Kawai, M. Soma, T. Onishi, K. Tamaru, Journal of Catalysis 62 (1980) 140–148.
[3] G.T. Went, L.-J. Leu, R.R. Rosin, A.T. Bell, Journal of Catalysis 134 (1992) 492–505.
[4] R. Burch, J.P. Breen, F.C. Meunier, Applied Catalysis B: Environmental 39 (2002) 283–303.
[5] R. Burch, T.C. Watling, Journal of Catalysis 169 (1997) 45–54.
[6] K. Eranen, F. Klingstedt, K. Arve, L.-E. Lindfors, D.Y. Murzin, Journal of Catalysis 227 (2004) 328–343.
[7] N. Macleod, R.M. Lambert, Applied Catalysis B: Environmental 35 (2002) 269–279.
[8] N. Macleod, R. Cropley, J.M. Keel, R.M. Lambert, Journal of Catalysis 221 (2004) 20–31.
[9] Y. Su, M.D. Amiridis, Catalysis Today 96 (2004) 31–41.
[10] H. Abdulhamid, E. Fridell, M. Skoglundh, Applied Catalysis B: Environmental 62 (2006) 319–328.
[11] A. Lindholm, H. Sjovall, L. Olsson, Applied Catalysis B: Environmental 98 (2010) 112–121.
[12] G. Carja, Y. Kameshima, K. Okada, C.D. Madhusoodana, Applied Catalysis B: Environmental 73 (2007) 60–64.
[13] X. Tang, J. Hao, H. Yi, J. Li, Catalysis Today 126 (2007) 406–411.
[14] O. Sun, W.M.H. Sachtler, Applied Catalysis B: Environmental 42 (4) (2003) 393–401.
[15] A. De Lucas, J.L. Valverde, F. Dorado, A. Romero, I. Asencio, Journal of Molecular Catalysis A: Chemical 225 (2005) 47–58.
[16] Z. Wu, B. Jiang, Y. Liu, Applied Catalysis B: Environmental 79 (2008) 347–355.
[17] T. Wang, K. Sun, Z. Lu, Y. Zhang, Reaction Kinetics, Mechanism and Catalysis 101 (2010) 153–161.
[18] Gongshin Qi, Ralph T. Yang, Applied Catalysis B: Environmental 44 (2003) 217–225.
[19] J. Huang, Z. Tong, W. Huang, J. Zhang, Applied Catalysis B: Environmental 78 (2008) 309–314.
[20] K. Eguchi, M. Watabe, S. Ogata, H. Arai, Bulletin of Chemical Society of Japan 68 (6) (1995) 1739–1745.
[21] M. Kang, E.D. Park, J.M. Kim, J.E. Yie, Catalysis Today 111 (2006) 236–241.
[22] B. Greenhalgh, J.-P. Charland, M. Stanciulescu, R. Burich, J. Kelly, Catalysis Today 15 (2010) 285–290.
[23] T. Maunula, Y. Kintaichi, M. Inaba, M. Haneda, K. Sato, H. Hamada, Applied Catalysis B: Environmental 15 (1998) 291–304.
[24] J. Kelly, M. Stanciulescu, J.-P. Charland, Fuel 85 (2006) 1772–1780.
[25] M.C. Biesinger, B.P. Payne, A.P. Grosvenor, L.W.M. Lau, A.R. Gerson, R.St.C. Smart, Applied Surface Science 257 (2011) 2717–2730.
[26] M.C. Biesinger, L.W.M. Lau, A.R. Gerson, R.St.C. Smart, Applied Surface Science 257 (2010) 887–898.
[27] H.W. Nesbitt, D. Banerjee, American Mineralogist 83 (1998) 305–315.
[28] H. Pan, Q. Su, J. Chen, Q. Ye, Y. Liu, Y. Shi, Environmental Science and Technology 43 (2009) 9348–9353.
[29] B. Greenhalgh, M. Fee, A. Dobri, J. Moir, R. Burich, J.-P. Charland, M. Stanciulescu, Journal of Molecular Catalysis A: Chemical 333 (2010) 121–127.
[30] J. Li, J. Chen, R. Ke, C. Luo, J. Hao, Catalysis Communications 8 (12) (2007) 1896–1900.
[31] A.E. Palomares, J.G. Prato, F.E.L. Imbert, A. Corma, Applied Catalysis B: Environmental 75 (2007) 88–94.
[32] K. Young Jin, K. Hyuk Jae, N. In-Sik, C. Jin Woo, K. Jeong Ki, K. Hong-Jip, C. Moon-Soon, Y. Gwon Koo, Catalysis Today 151 (2010) 244–250.
[33] G. Qi, R.T. Yang, Journal of Catalysis 217 (2003) 434–441.
[34] B. Guan, H. Lin, L. Zhu, Z. Huang, Journal of Physical Chemistry C 115 (26) (2011) 12850–12863.
[35] S.H. Park, B.H. Kim, M. Selvaraj, T.G. Lee, Journal of Industrial and Engineering Chemistry 13 (4) (2007) 637–643.
[36] P.S. Metkar, N. Salazar, R. Muncrief, V. Balakotaiah, M.P. Harold, Applied Catalysis B: Environmental 104 (2011) 110–126.
[37] F. Liu, H. He, Y. Ding, C. Zhang, Applied Catalysis B: Environmental 93 (2009) 194–204.